The earliest phases of star formation: From low– to high–mass objects

Proposal for a Herschel-PACS GT Key Project

O. Krause, Th. Henning, H. Beuther, S. Birkmann, M. Hennemann, R. Launhardt, D. Lemke, H. Linz, M. Nielbock, J. Steinacker (all MPIA Heidelberg), R. Klein (MPE Garching), B. Stecklum (TLS Tautenburg), and P. André (CEA Saclay)

It is generally agreed that present–day Galactic star formation starts in the coldest and densest cores of molecular clouds. However, our knowledge about the very early stages of star formation is still quite limited. Such objects emit most of their luminosity at far–infrared wavelengths (roughly 60 – 400 μm), thus not (or not easily) observable from the ground. Hence, up to now our view in this wavelength range remains fuzzy at best, since all available information generally come from small aperture satellite and airborne missions which severely lack spatial resolution. This is a major drawback for detailed studies of young low–mass cores, and it has severely hampered almost any progress in identifying and thoroughfully characterising young and cold high–mass cores which are, on average, far more distant. Still, detailed knowledge about these early pre– and proto–stellar stages is indispensable if we want to answer fundamental questions about the physics of the early collapse phase, the core fragmentation and the principle ways to finally form stars of all masses. With the advent of the Herschel satellite, we will have the unique opportunity to deeply scrutinise such cold cradles of stars with unprecedented sensitivity and angular resolution. We therefore propose to use the PACS and SPIRE instruments to perform deep and directed multi-wavelength mapping of individual objects and confined regions. We have compiled a unique sample of low– and high–mass targets that we identified, based on careful preparatory studies (including ISO and Spitzer observations), as very promising sources for the study of initial conditions of star formation. The Herschel data will allow us to reconstruct the (3D) density and temperature structure, to assess the energy budget of the cores and to unveil potential substructures. Furthermore, Herschel observations will render it possible for the first time to perform an advanced modelling of such cold cores that is meaningful and not plagued by simplifications and parameter ambiguities.

Propsal Overview and Science Goals

The proposal includes two different target groups that require slightly different observing strategies: 1) isolated low-mass prestellar cores and protostars in regions of exceptionally low cirrus noise and 2) candidates of high-mass prestellar and protostellar cores.

We will derive in detail the properties, in particular temperature and density structure, of individual pre-identified low- and high-mass prestellar cores and protostellar envelopes. This will be accomplished by deep pointed observations of selected targets in contrast to (shallow) blind surveys of large areas.

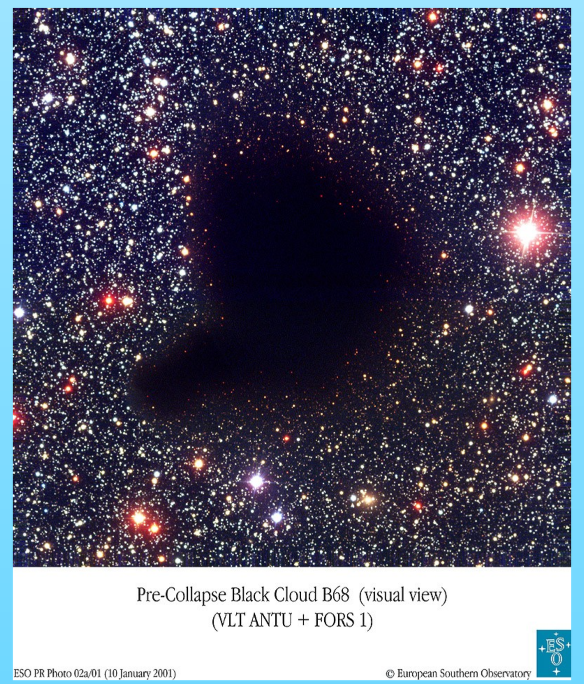

The targeted low mass cores will be observed with PACS and SPIRE and the data will be combined with existing ground-based (sub)mm maps. From the spatially resolved flux ratios we will measure the dust temperature distribution with an accuracy of $\Delta T < 1$K and derive density profiles and the mass distribution. This will yield constraints on external heating (energy input from the ISRF), internal heating and the dust properties. By means of radiative transfer modelling the data will allow a precise quantification of the initial conditions of isolated star formation.

▲ Prestellar core B68
gas/dust temperature ~10K
mass 3 M☉
diameter 0.1 pc
linewidth 0.2 km s^{-1}
distance 120 pc

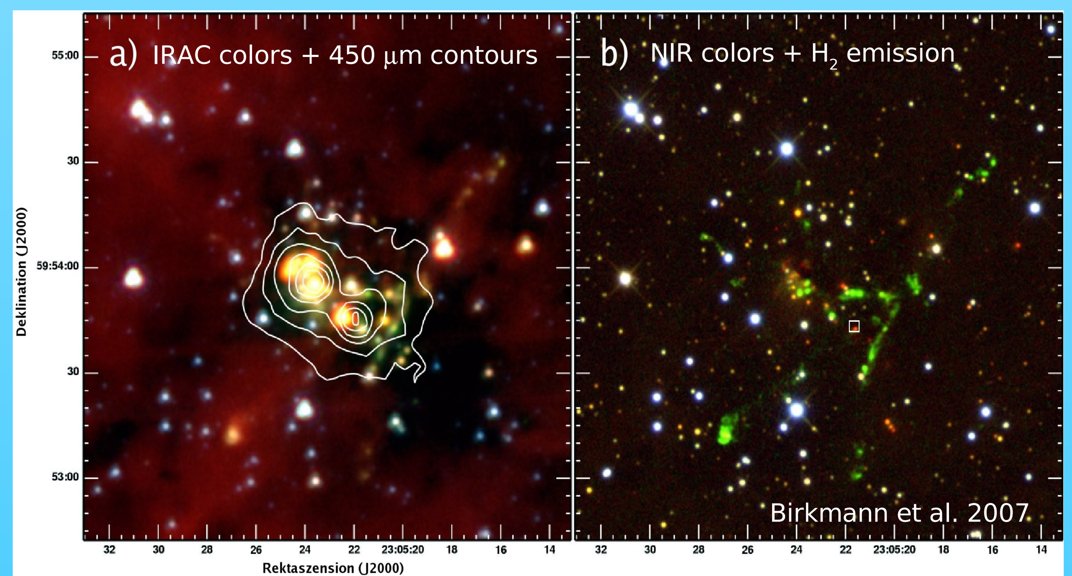

Massive SFR ISOSS 23053+5953
gas/dust temperature ~15K
mass 1000 M☉
distance 3.5 kpc ▶

The main goal for the more complex high-mass star forming regions (SFRs) is to unambiguously identify and, for the first time, comprehensively characterise the prestellar stages of massive star birth. In addition the PACS and SPIRE observations, combined with an extensive set of existing multi-wavelength data, will allow to study potential fragmentation of the high-mass cores and put constraints on external/internal heating and dust properties by means of radiative transfer modelling. Furthermore embedded low-mass objects down to ~ 0.3 M☉ will be detected.

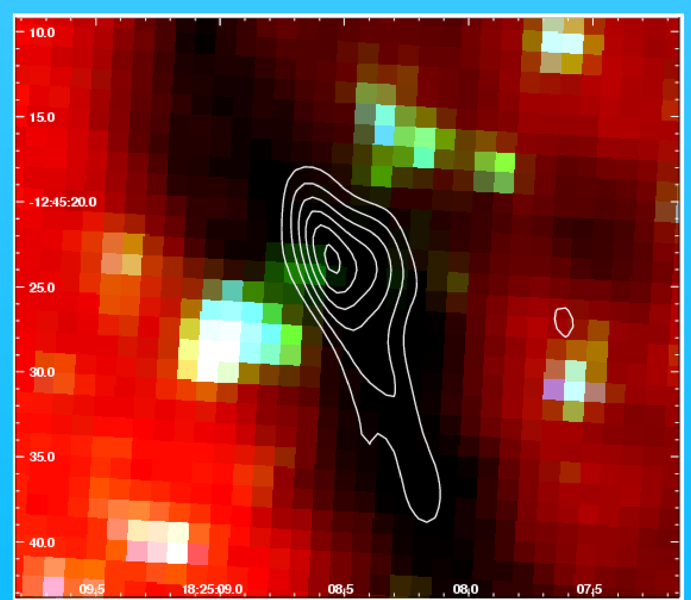

IRAC 3-color composite + 1.2 mm contours (Beuther et al. 2005)

The infrared dark cloud IRDC18223-3 is a massive mm-continuum gas core without a MIR counterpart. The green 4.5 μm emission indicates molecular outflows (supported by CO and CS line observations) and suggests the onset of massive star formation. The early evolutionary state of this object is supported by the cold dust temperatures in the envelope as derived from its SED. The proposed PACS and SPIRE observations will fully cover the so far unobserved spectral range at and around the peak of the thermal emission with high spatial resolution.

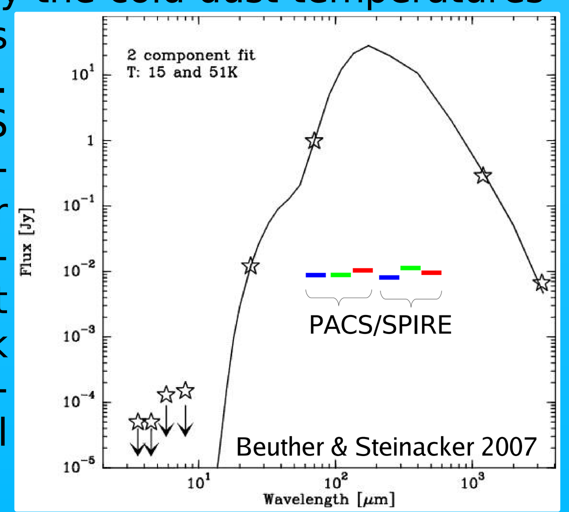

Target Selection

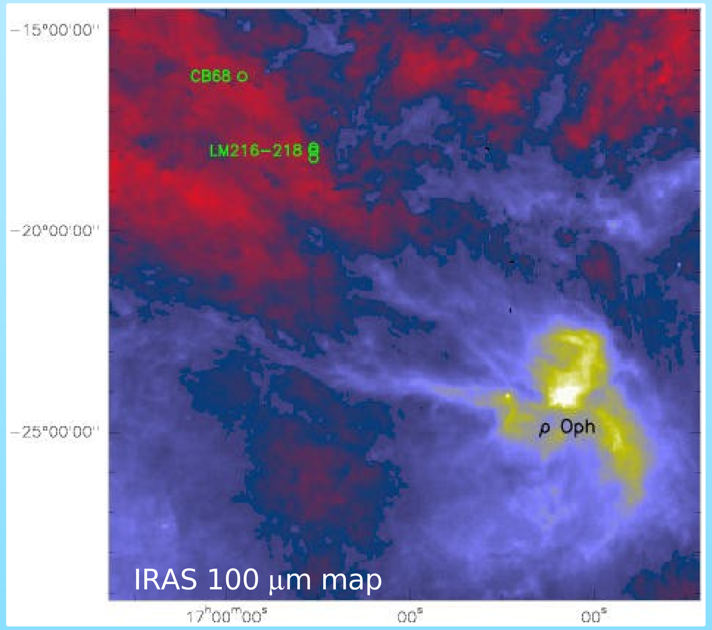

For the low-mass case we selected 20 targets of isolated prestellar and protostellar cores in regions of exceptionally low cirrus confusion noise (< 1 mJy/beam at 110 μm). Only known and well-studied sources were considered. Their distances range between 140 and 300 pc, yielding a linear resolution of about 1000 (@110 μm) to 7000 AU (@350 μm).

DSS2
+ IRAS 100 μm
+ mm contours

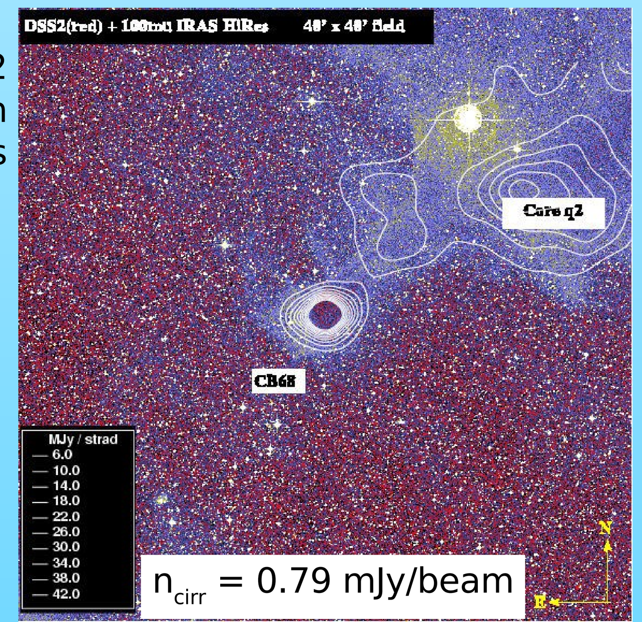

The sample of high-mass SFR were selected from MPIA surveys of well studied sources, that have an extensive set of existing multi-wavelength data. The samples were build up using different selection techniques, with the common goal of identifying candidates for massive star forming regions in an early evolutionary state: by using the ISOPHOT Serendipity Survey (ISOSS) and by selecting high-mass starless cores (HMSCs) and infrared dark clouds (IRDCs).

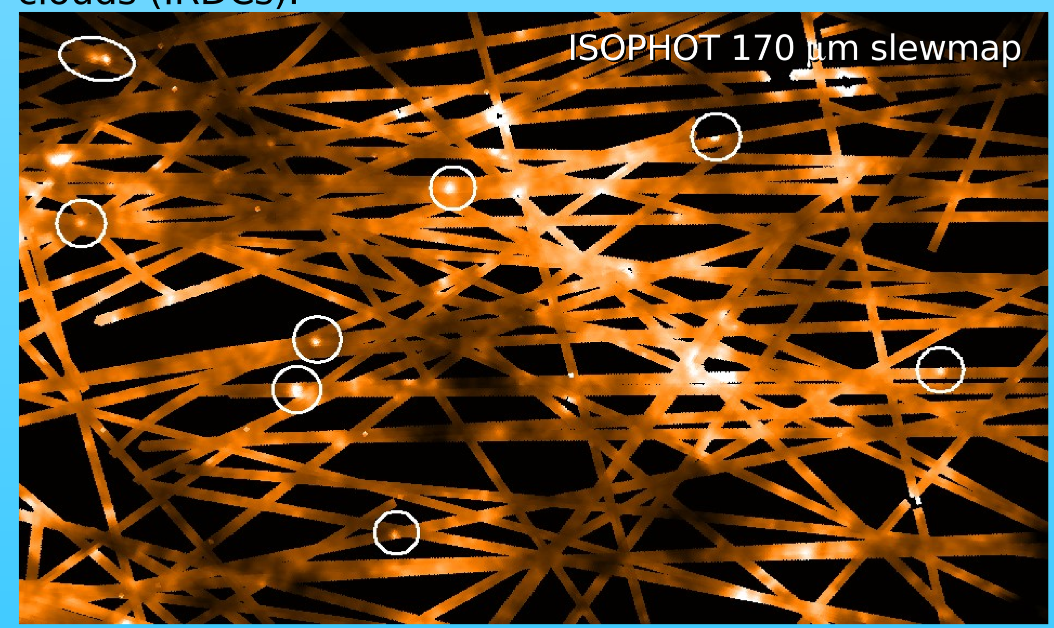

▲ ISOSS slew-map with young SFRs candidates marked

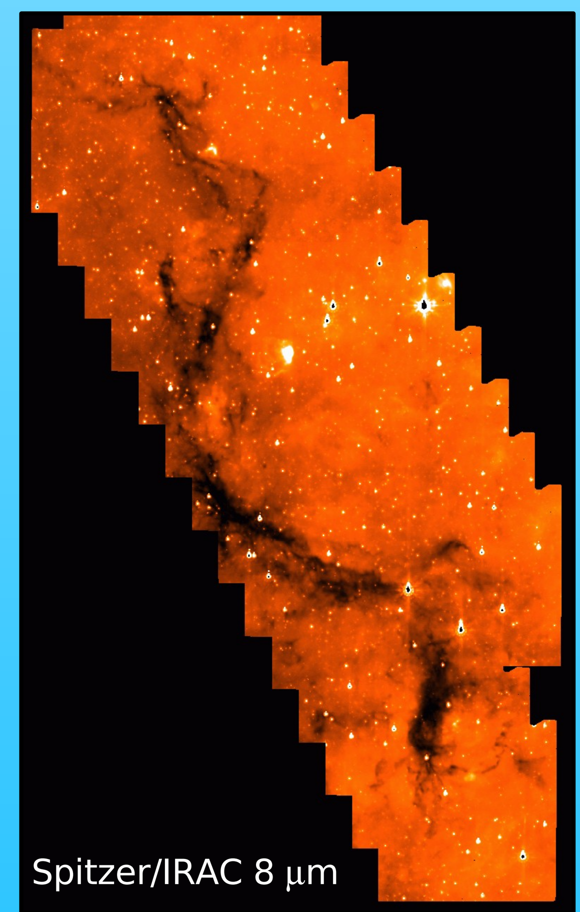

IRDC complex G11.11-0.12

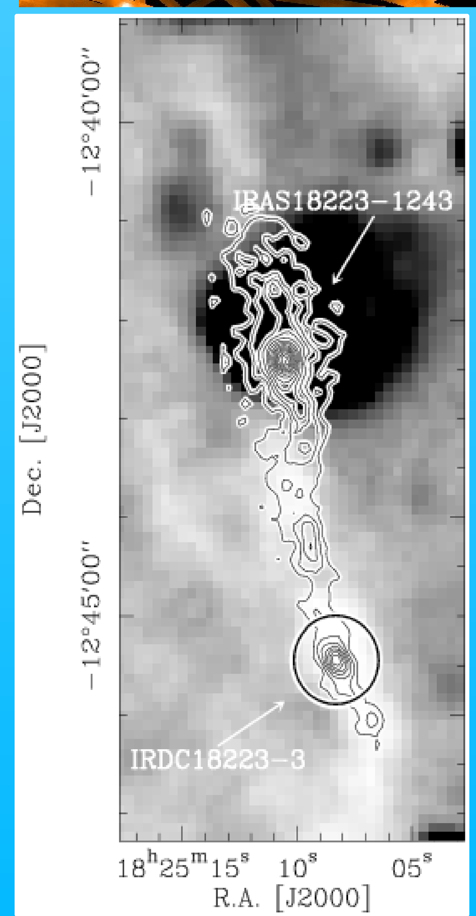

◀ The mm-only core IRDC 18223-3

grey scale: MSX 8 μm
cotours: 1.2 mm

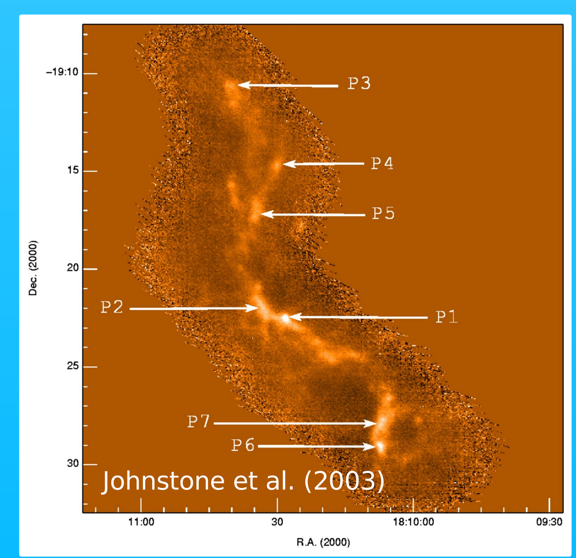

SCUBA 850 μm continuum

Observing Strategy and Target Lists

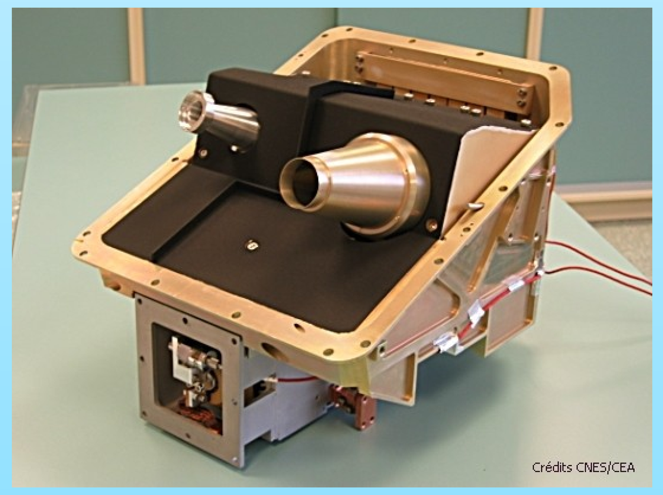

The flight model of the PACS bolometer camera manufactured by CEA. Below the layout of the two arrays that allow for simultaneous imaging in two of the three photometric bands of PACS is shown.

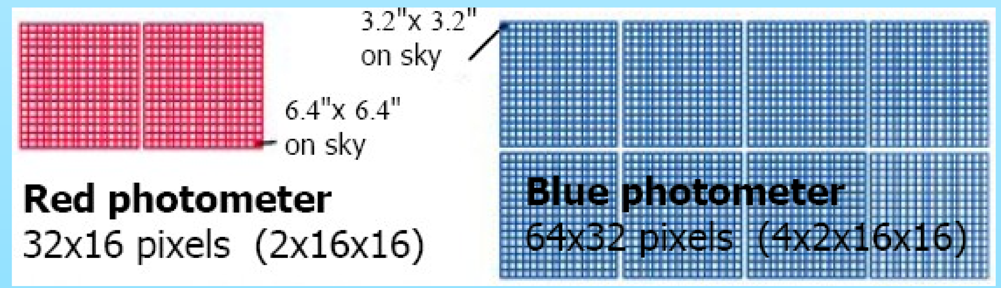

	Low-mass SFRs	High-mass SFRs
Bands	110 μm & 170 μm	70 μm, 110 μm & 170 μm
	250 μm, 350 μm (& 500 μm)	250 μm, 350 μm & 500 μm
Map size	6x6 to 10x10 arcmin² scan map (adapted to source size)	6x6 to 4x14 arcmin² scan map (adapted to source morphology)
	4x4 arcmin² jiggle map	6x6 to 4x14 arcmin² scan map
Detection Limit (point source)	2 mJy/beam (1-σ) (close to confusion noise limit @ 110 μm)	10 mJy/beam (1-σ) (close to confusion noise limit @ 110 μm)
	4 mJy/beam (1-σ)	10 mJy/beam (1-σ)
Time estimate	2 – 6.7 hrs per map	28 min (6x6 arcmin²)
	15 min	15 min (6x6 arcmin²)
# of targets	≤ 20 (≤ 60 hrs total)	≈ 70 (48 hrs total)

The proposed observing strategies with PACS and SPIRE for the selected low- and high-mass star forming regions.

Target lists for the low- (bottom left) and high-mass SFRs (bottom right). For the low-mass case the list is not fully finalized, but all candidate regions are displayed. For the high-mass SFRs only a partial listing of the targeted IRDCs is shown, due to the larger number of sources.

Source Name	RA (2000)	Dec (2000)	Dist. [pc]	Evol. Stage	PSCN(110)† [mJy/beam]	MapSize [arcmin]	Remark	Pr.*
CB 4	00 : 39 : 03	+52 : 51 : 30	200	PPS	0.48	6x6	–	A
CB 17	04 : 04 : 38	+56 : 56 : 12	300	PPS	0.73	6x6	–	A
L 1521 F	04 : 28 : 39	+26 : 51 : 36	140	PPS	0.71	10x10	1, 2	A
CB 23	04 : 43 : 32	+29 : 40 : 00	140	PPS	0.66	6x6	–	B
L 1517B2	04 : 55 : 08	+30 : 42 : 49	140	PPS	0.63	8x6	–	A
CB 27	05 : 04 : 09	+32 : 43 : 08	140	PPS	0.72	6x6	–	B
L 1544	05 : 04 : 16	+25 : 10 : 48	140	PPS	0.63	10x10	1, 2	A
L 260	16 : 46 : 58	−09 : 36 : 20	165	PPS	0.98	6x6	–	B
L 63	16 : 50 : 14	−18 : 05 : 59	165	PPS	0.78	8x6	–	A
CB 222	20 : 33 : 31	+64 : 01 : 24	400	PPS	0.43	6x6	–	B
B 68	17 : 22 : 35	−23 : 49 : 30	160	PPS	2.02	6x6	–	C
CB 130	18 : 16 : 15	−02 : 32 : 48	200	PPS	2.12	6x6	–	C
CB 246	23 : 54 : 05	+58 : 17 : 59	140	PPS	1.22	8x4	–	C
IRAM 04191	04 : 21 : 56	+15 : 29 : 46	140	Cl0	0.66	6x6	1	A
L 1582B	05 : 32 : 37	+27 : 08 : 35	400	Cl0	0.85	6x6	–	B
CB 68	16 : 57 : 16	−16 : 09 : 18	160	Cl0	0.79	6x6	–	A
B 335	19 : 36 : 55	+07 : 34 : 24	250	Cl0	0.66	6x6	–	A
CB 232	21 : 37 : 14	+43 : 21 : 30	600	Cl0	0.85	6x6	–	B
CB 244	23 : 25 : 47	+74 : 17 : 36	180	Cl0	0.39	8x6	–	A
L 723	19 : 17 : 52	+19 : 12 : 14	300	Cl0	2.08	6x6	–	C
IRAS 03282	03 : 31 : 20	+30 : 45 : 24	300	Cl0	1.12	6x6	–	C
BHR 12	08 : 09 : 33	−36 : 05 : 00	200	Cl0	1.45	6x6	–	C
BHR 36	08 : 25 : 44	−51 : 02 : 06	400	Cl0	1.4	6x6	–	C
CB 6	00 : 49 : 29	+50 : 44 : 36	200	Cl1	0.31	6x6	–	B
CB 26	05 : 00 : 09	+52 : 04 : 54	140	Cl1	0.68	6x6	–	A
BHR 86	13 : 07 : 38	−77 : 00 : 21	200	Cl1	0.51	6x6	–	B
CB 230	21 : 17 : 39	+68 : 17 : 32	400	Cl1	0.85	6x6	–	A
CB 180	19 : 06 : 22	−06 : 54 : 08	200	Cl1	1.11	8x6	–	C

Name	R.A. J2000	Dec. J2000	D kpc	$v(H^{13}CO^+)$ km s^{-1}	$\Delta v(NH_3)$ km s^{-1}	$T(NH_3)$ K	$\Delta v_0(SiO)^e$ km s^{-1}	$S^g_{1.2mm}$ Jy	M^g M☉	$S^h_{1.2mm}$ $\frac{mJy}{(11'')^2}$	$N^h_{H_2}$ 10^{23}cm^{-2}	Prio.	Size
IRDC18089−1732-3	18 11 45.3	−17 30 38	3.6	34.2(0.1)	2.2	15.6	5.5	0.3	241	147	1.5	B	
IRDC18090−1832-2	18 12 02.0	−18 31 27	6.6	111.2(0.1)				0.2	541	89	0.9	C	
IRDC18102−1800-1	18 13 11.0	−18 00 23	2.7	21.4(0.1)			42.2	3.3	1385	632	6.3	B	
IRDC18151−1208-2	18 17 50.3	−12 07 54	3.0	29.8(0.1)	2.2	18.5	65.0	2.6	1453	620	6.2	A	
IRDC18182−1433-2	18 21 14.9	−14 33 06	3.6	40.9(0.1)	1.4	15.5		0.3	241	144	1.4	B	
IRDC18182−1433-3	18 21 17.5	−14 29 43	4.6	60.2(0.1)	1.2		5.5					B	
IRDC18182−1433-4	18 21 14.0	−14 34 20	3.6	41.4(0.1)								B	
IRDC18223−1243-2	18 25 10.0	−12 44 00	3.7	45.5(0.1)				0.6	510	156	1.6	A	14′ × 4′^{a}
IRDC18223−1243-3	18 25 08.3	−12 45 27	3.7	45.7(0.1)	2.2	32.7	35.5	0.8	686	289	2.9	A	14′ × 4′^{a}
IRDC18223−1243-4	18 25 06.8	−12 48 00	3.7	45.7(0.1)	1.4	13.0	38.9	0.3	255	77	0.8	A	14′ × 4′^{a}
IRDC18223−1243-5	18 25 12.0	−12 53 23	3.7	45.1(0.2)	1.1							A	14′ × 4′^{a}
IRDC18223−1243-6	18 25 16.2	−12 55 33	3.7	45.7(0.1)	1.4		2.4					A	14′ × 4′^{a}
IRDC18223−1243-6	18 25 16.2	−12 55 33	3.7	50.9(0.2)	2.1							A	14′ × 4′^{a}
IRDC18247−1147-3	18 27 31.0	−11 44 46	6.7	59.7(0.2)				0.4	1115	110	1.1	B	
IRDC18306−0835-3	18 33 32.1	−08 32 28	3.8	54.8(0.1)	1.6	13.1		0.8	310	154	1.5	A-	^{a}
IRDC18306−0835-4	18 33 34.8	−08 31 20	3.8	55.2(0.1)	2.0							A-	^{a}
IRDC18308−0841-3	18 33 29.3	−08 38 17	4.9	-	1.9	16.2	-	0.7	1044	102	1.0	B	
IRDC18308−0841-5	18 33 34.4	−08 37 36	4.9	-	1.5	14.5	-	0.2	298	78	0.8	B	
IRDC18310−0825-4	18 33 39.5	−08 21 10	5.2	-	1.7	18.3	-	0.5	840	132	1.3	A-	
IRDC18337−0743-3	18 36 18.2	−07 41 00	4.0	56.2(0.1)	1.8	15.6	39.8	0.3	298	123	1.2	A	
IRDC18337−0743-4	18 36 29.9	−07 42 05	4.0	55.8(0.1)	2.1							C	
IRDC18337−0743-5	18 36 41.0	−07 39 56	4.0	58.4(0.1)			16.2					C	
IRDC18337−0743-6	18 36 36.0	−07 42 17	4.0	56.6(0.1)								C	
IRDC18337−0743-7	18 36 19.0	−07 41 48	4.0	55.9(0.1)								C	
IRDC18348−0616-2	18 37 27.6	−06 14 08	6.3	109.7(0.1)			9.9	0.5	1232	169	1.7	B	
IRDC18348−0616-8	18 37 14.7	−06 17 25	6.3	109.3(0.2)								C	
IRDC18385−0512-3	18 41 17.4	−05 10 03	3.3	47.0(0.1)	1.1	14.4	41.1	0.3	344	77	0.8	A	
IRDC18431−0312-3	18 45 45.0	−03 08 56	6.6	105.4(0.3)								C	
IRDC18431−0312-4	18 45 53.0	−03 09 01		non det.								C	
IRDC18437−0216-3	18 46 21.9	−02 12 24	6.2	97.6(0.2)	1.2	15.9		0.3	811	96	1.0	A-	^{a}
IRDC18437−0216-3	18 46 21.9	−02 12 24	7.3	111.3(0.1)	1.4	15.9		0.3	811	96	1.0	A-	^{a}
IRDC18437−0216-7	18 46 22.0	−02 14 10	6.2	96.1(0.1)			13.0					A-	^{a}
IRDC18437−0216-7	18 46 22.0	−02 14 10	7.3	111.2(0.7)								A-	^{a}
IRDC18440−0148-2	18 46 31.0	−01 47 08	5.6	97.9(0.2)								C	
IRDC18445−0222-4	18 47 14.6	−02 15 44		-	1.0		-					C	
IRDC18447−0229-3	18 47 42.0	−02 25 12	6.4	102.1(0.2)	1.1							B	
IRDC18447−0229-4	18 47 38.9	−02 28 00	6.4	99.4(0.1)	1.3							B	

References

Beuther et al. 2005, ApJL 634, L57
Beuther & Steinacker 2007, ApJL, 656, L85
Birkmann et al. 2007, accepted for publication in A&A
Johnstone et al. 2003, ApJL, 588, L37